BIOCHEMISTRY
including biophysical chemistry & molecular biology
Article

Biochemistry **2010,** *49,* 2051–2057 2051
DOI: 10.1021/bi9020007

Energy Transfer Ligands of the GluR2 Ligand Binding Core†

Amy F. Petrik, Marie-Paule Strub, and Jennifer C. Lee*

Laboratory of Molecular Biophysics, National Heart, Lung, and Blood Institute, National Institutes of Health, 50 South Drive, Bethesda, Maryland 20892

Received November 20, 2009; Revised Manuscript Received January 26, 2010

ABSTRACT: Ionotropic glutamate receptors (iGluRs) are ligand-gated ion channels that mediate excitatory signaling in the central nervous system. When a ligand binds to the extracellular domain of iGluRs, local conformational changes ensue and this motion is translated to the transmembrane domain, inducing channel opening. We have used an isolated ligand binding domain, GluR2-S1S2J (GluR2), as a model system to study the protein−ligand complex by steady-state and time-resolved intrinsic tryptophan fluorescence measurements. Specifically, we determined that the widely used and structurally characterized antagonist, 6,7-dinitroquinoxaline-2,3-dione (DNQX), acts as an efficient fluorescence energy transfer (FET) acceptor for Trp. Consistent with crystallographic data, our results indicate that the four native tryptophans are within Förster's radius ($R_o \sim 33$ Å) of the bound ligand. Additionally, we demonstrate the broader value of this technique by identifying an original FET ligand, 3-nitrotyrosine (3NY), for GluR2 ($R_o \sim 24$ Å; apparent dissociation constant $K_d \sim 170$ μM). Estimated average donor−acceptor (Trp−ligand) distances extracted from tryptophan excited-state decays are similar for both ligands (~24 Å), suggesting that 3NY binds in the structurally characterized ligand binding cleft. Moreover, an alternative competition assay utilizing Trp → DNQX quenching for detection of ligand binding in GluR2 is described.

Ionotropic glutamate receptors (iGluRs),[1] a family of ligand-gated ion channels, mediate fast excitatory signaling in the central nervous system (CNS) by coupling neurotransmitter or ligand binding to ion channel opening (*1*, *2*). iGluRs assemble as a heterotetramer with a central pore formed by the transmembrane domains that opens as a cation-permeable channel in response to ligand binding (*3*). There are three distinct classes of glutamate receptors based on their relative affinities for the ligands: *N*-methyl-D-aspartic acid (NMDA), α-amino-3-hydroxy-5-methyl-4-isoxazolepropionic acid (AMPA), and kainate. These proteins are widely expressed in the CNS and are thought to be essential to processes of learning and memory by enabling synaptic plasticity (*3*, *4*). Dysfunction of iGluRs is associated with neuronal disorders, including epilepsy and stroke (*5*, *6*).

GluR2 is categorized as an AMPA receptor (*2*) and binds AMPA with nanomolar affinity (*7*). It is comprised of the extracellular amino-terminal (ATD) and ligand binding domains (LBD) as well as three transmembrane helices and one reentrant loop (Figure 1, right panel). Upon binding, a ligand can induce a conformational change in the LBD that is hypothesized to propagate to the transmembrane domain and result in opening of the ion channel (*2*). A recombinant form of the isolated LBD, GluR2-S1S2J (here termed GluR2) (*8*), cloned from *Rattus norvegicus*, has allowed for extensive structural characterization of the ligand−protein complex (Figure 1, left panel) (*7*, *9*−*13*). The crystallographic structure shows that the LBD is formed by two lobes with the ligand binding site situated at the cleft between them. With a ligand bound, the two domains approach one another, closing around the ligand in what is termed a clamshell structure (*13*). The extent to which opening occurs is closely correlated with the activity of the ligand on the ion channel. Agonists, which cause the channel to open, induce the LBD to close tightly around them (*14*), while structures

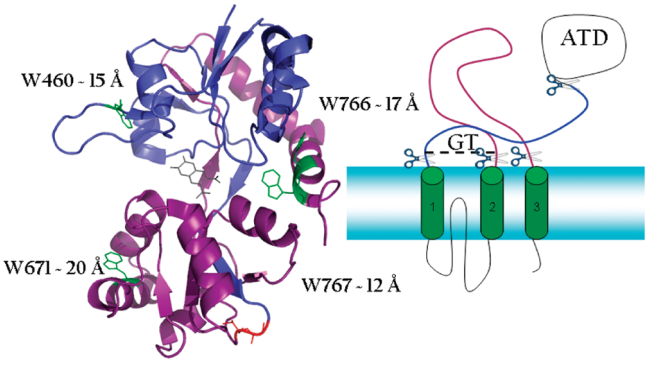

FIGURE 1: Structures of GluR2-S1S2J. The left panel shows backbone atoms of DNQX-bound GluR2 (PDB entry 1FTL) (*16*) shown as a ribbon structure with the S1 domain colored blue, the S2 domain purple, and the dipeptide linker (GT) red. This structure has been described as a clamshell with the ligand binding site between two lobes that close around the ligand upon binding. The four native tryptophan fluorophores (Trp 460, 671, 766, and 767) and their respective distances from DNQX are highlighted. The right panel shows a schematic representation of the full-length protein, including three transmembrane helices (numbered 1−3), a reentrant loop, and an amino-terminal domain (ATD) that have been removed in the ligand binding domain construct used in this study (*38*).

†This work is supported by the Intramural Research Program of the National Institutes of Health, National Heart, Lung, and Blood Institute.

*To whom correspondence should be addressed. E-mail: leej4@mail.nih.gov. Telephone: (301) 496-3741. Fax: (301) 402-3404.

[1]Abbreviations: iGluR, ionotropic glutamate receptor; CNS, central nervous system; GluR2, isolated ligand binding domain GluR2-S1S2J; AMPA, α-amino-3-hydroxy-5-methyl-4-isoxazolepropionic acid; ATD, amino-terminal domain; LBD, ligand binding domain; 3NY, 3-nitrotyrosine; DNQX, 6,7-dinitroquinoxaline-2,3-dione; FET, fluorescence energy transfer; NATA, *N*-acetyltryptophanamide; PDB, Protein Data Bank.

Published on Web 02/15/2010

containing antagonists or receptor inhibitors appear to closely resemble the apoprotein (*15*). It has been suggested that the antagonists essentially "prop open" the two lobes of the ligand binding domain, preventing the channel from opening (*16*−*18*).

Competition radioligand assays have been widely used to identify and determine potential ligands (*8*). Though requiring minimal amounts of material, this method does necessitate the use of radioactivity that employs special equipment and safety precautions which may not be available in all laboratories. In addition, the choice of commercially available radioligands can be limited, and the use, as well as disposal, of compounds poses environmental and economical concerns. Alternatively, intrinsic fluorescence arising from aromatic tryptophan and tyrosine residues of GluR2 has been utilized to detect ligand binding events (*2*, *13*). Addition of the naturally occurring ligands, AMPA, glutamate, and kainate, results in modest quenching of the protein emission (10−15% at saturating ligand concentrations). Because of this notably low dynamic range, a high rate of repetition of measurements is necessary to obtain reliable results. Nevertheless, intrinsic fluorescence measurements have proven to be successful in identifying and characterizing new ligands (*19*, *20*).

While the amino acid tryptophan is a natural fluorophore (*21*−*23*) that has been used as a local reporter (emission spectrum and quantum yield) of solvent polarity and the local environment formed by nearby amino acid residues, tryptophan also can be utilized as a polypeptide conformational probe (*24*−*27*). In our approach, we exploited the four intrinsic Trp residues (Figure 1, left panel, PDB entry 1FTL) (*16*) as fluorescence energy transfer (FET) donors (*21*, *28*, *29*) to identify potential energy acceptor ligands; FET measurements allow for the site-specific structural determination of the distance between a donor fluorophore and an acceptor molecule based on the efficiency of FET [inversely dependent on the donor−acceptor separation (R_{DA}) to the sixth power]. Specifically, we employed time-resolved fluorescence spectroscopy to directly assess FET rates, eliminating complications from steady-state measurements such as direct excitation of the acceptor (if using a fluorescent acceptor) and the inner filter effect. Applying this method and using low protein concentrations (micromolar), we determined that both a known antagonist, DNQX, and a new ligand, 3-nitrotyrosine (3NY), can act as FET acceptors for the Trp residues of GluR2. Additionally, we report here for the first time the time-resolved characteristics of the Trp residues in GluR2 and use these measurements to estimate protein−ligand distances.

EXPERIMENTAL PROCEDURES

Materials. All reagents were obtained from Sigma-Aldrich (St. Louis, MO), except 3-nitrotyrosine which was purchased from Cayman Chemicals (Ann Arbor, MI), and were used as received.

Protein Expression and Purification. The GluR2 expression plasmid was generously provided by E. Gouaux (The Vollum Institute, Oregon Health & Science University, Portland, OR) (*8*). The protein was expressed and purified using protocols similar to those developed by Gouaux and co-workers (personal communication). Briefly, Origami B cells (Novagen, Darmstadt, Germany) expressing GluR2 (36 g) were resuspended in 20 mM Tris buffer (pH 8.0, 150 mL) containing 150 mM NaCl, 1 mM $MgSO_4$, 5 mM methionine, 1 mM glutamate, 50 μg/mL lysozyme, and EDTA-free protease inhibitor cocktail (Roche, Indianapolis, IN) and lysed using a high-pressure cell disruptor (Avestin, Mannheim, Germany). Following centrifugation [4500 rpm in a SLC-4000 rotor (Sorvall, Waltham, MA) for 45 min] and ultracentrifugation [35000 rpm in a Ti45 rotor (Beckman, Fullerton, CA) for 1 h] steps, the supernatant was loaded onto a HisPrep 16/10 affinity chromatography column (GE Healthcare Lifesciences, Piscataway, NJ) and protein was eluted with an imidazole gradient (from 0 to 400 mM, 20 mM Tris buffer, pH 8.0). Fractions containing GluR2 were pooled, and the N-terminal His tag was removed by thrombin cleavage at room temperature (100 units for 2 h). The protein was dialyzed against 20 mM HEPES buffer (pH 7.0) containing 1 mM glutamate and 5 mM methionine and further purified on a MonoS cation exchange column (0 to 1 M NaCl gradient). All dialysis and chromatographic steps were performed at 4 °C. Fractions of purified protein were dialyzed extensively (at least three changes into at least 100 times of starting volume each time) against 10 mM HEPES buffer (pH 7.0) containing 20 mM NaCl and 1 mM EDTA to remove bound glutamate (estimated residual Glu concentration of ≤10 pM). The purity of all protein samples was assessed by SDS−PAGE analyses. Protein concentrations were determined using a molar extinction coefficient estimated on the basis of amino acid content (ε_{280} = 41370 M^{-1} cm^{-1}). All purified proteins were concentrated using a Centriprep YM-10 device (molecular mass cutoff of 10 kDa, Millipore, Billerica, MA) and stored at −80 °C. The protein molecular mass and folded structure were confirmed by ESI-MS (30302 mass units measured, 30302 calculated) and CD spectra ($[\Theta]_{222}$ = −10 mean molar ellipticity per residue), respectively. Absorption, fluorescence, and CD spectra were recorded on a CARY 300 Bio UV−vis spectrophotometer (Varian, Santa Clara, CA), a Fluorolog-3 spectrofluorimeter (Horiba Jobin Yvon, Edison, NJ; λ_{ex} = 295 nm, λ_{obs} = 300−450 nm, 0.25 s integration time, 1 nm excitation and emission slit widths), and a Jasco J-715 spectropolarimeter (Jasco, Easton, MD; 180−300 nm, 2 nm steps, 1 nm bandwidth, 0.5 s integration time, 50 nm/min), respectively.

Time-Resolved Fluorescence Measurements. Time-resolved fluorescence measurements were taken using excitation (293 nm, 1 kHz, 0.025−0.10 mW) from harmonic generation of an optical parametric amplifier (Light Conversion) pumped by a regeneratively amplified Ti:sapphire laser (Clark MXR, Dexter, MI). Trp emission was collected under magic angle conditions selected through a 340 ± 10 nm filter (CVI, Albuquerque, NM) with an array of optical fibers. A streak camera (Hamamatsu C5680, Hamamatsu, Bridgewater, NJ) was operated in single-photon counting mode and used to measure decay kinetics (at least 10^4 counts were accumulated in the peak channel, typical collection time of 5−10 min).

Ligand solutions were prepared in buffer immediately prior to experiments, and concentrations were determined gravimetrically and confirmed spectrophotometrically when possible [ε_{335}(DNQX) = 23400 M^{-1} cm^{-1}, and ε_{340}(3NY) = 3300 M^{-1} cm^{-1}]. Protein/ligand solutions were prepared, added to cuvettes, and deoxygenated by repeated evacuation and Ar gas fills on a Schlenk line over a period of 45 min. All measurements were taken at 25 °C using a temperature-controlled cuvette holder. Measurements of steady-state emission spectra before and after laser experiments showed negligible photobleaching (< 10%).

Competition Assay. The competition assays were conducted by monitoring GluR2 (1 μM GluR2) emission at a wavelength of

340 nm (5 nm slit width, λ_{ex} = 295 nm) with constant stirring using a PTI (Princeton, NJ) Quantamaster fluorimeter. For every measurement, the emission of protein alone (10 mM HEPES, 20 mM NaCl, 1 mM EDTA, and pH 7.0 buffer) was measured for 100 s to ensure sample integrity. The sample was allowed to equilibrate with 1 equiv of DNQX (1 μL of a 1 mM DNQX solution), the FET ligand. The reduced emission from the GluR2−DNQX complex was monitored for at least 100 s to ensure signal stability before competitive ligand additions. Subsequently, additions of non-FET ligands (2 μL of concentrated 20 μM glutamate) were added every 100 s, and the emission was measured. The average emission intensity for each solution condition was determined and plotted versus the concentration of competitive ligand added.

DATA ANALYSIS

Ligand Binding Curves. The fluorescence intensity for each sample was calculated by integrating the area from 300−450 nm for the steady state and under the peak-normalized emission curve [$I(t = 0) = 1$] for time-resolved data. The proportion of quenching was calculated by dividing by the emission intensity for the protein sample without ligand present.

Plots of fractional quenching as a function of ligand added [$Q(L)$] were constructed and fit using the Hill equation (eq 1) in Igor Pro (Wavemetrics, Oswego, OR):

$$Q(L) = Q(L = \infty) + \frac{Q(L = 0) - Q(L = \infty)}{1 + \left(\frac{K_d}{L}\right)^n} \quad (1)$$

where L is the ligand concentration, $Q(L = 0)$ and $Q(L = \infty)$ are the relative fluorescence intensities in the absence and presence of saturating ligand concentrations, respectively, n is the Hill coefficient, and K_d is the apparent dissociation constant for the interaction between the ligand and protein. The Hill coefficient (n) was held to a value of 1.

R_o Calculation. The Förster radii for the tryptophan residues in GluR2 and the two energy transfer ligands were calculated using eq 2:

$$R_o = \left(\frac{8.8 \times 10^{-25} \times \kappa^2 \Phi_D J}{\eta}\right)^{1/6} \quad (2)$$

where κ^2 is the dipole orientation factor which we took to be $^2/_3$ assuming complete rotational freedom of the tryptophan residues, η is the refractive index of the solution, Φ_D is the quantum yield of the donor in the absence of the acceptor, and J is the overlap integral between the donor emission spectrum and the acceptor absorption spectrum. The calculation of J is given by eq 3.

$$J = \int_{-\infty}^{\infty} I_d(\lambda)\varepsilon_a(\lambda)\lambda^4 \, d\lambda \quad (3)$$

where I_d is the relative emission intensity of the donor and ε_a is the absorption spectrum of the acceptor.

Fluorescence Decay Kinetics. The fluorescence decay kinetics were modeled with eq 4 to account for the nonexponential behavior typically exhibited by tryptophan fluorophores in protein (*24*, *26*, *30*).

$$I(t) = I_0(t) \int P(k_{FET}) e^{-k_{FET}(R)t} \, dk_{FET} \quad (4)$$

where $P(k_{FET})$ is the probability of observing a protein conformation with a rate constant $k_{FET}(R)$ for distance R and $I_0(t)$ is the Trp fluorescence decay of apo-GluR2 (no ligand) in the absence of energy transfer to DNQX or 3NY. Donor−acceptor distance distributions were calculated from the decay kinetics by numerical inversion of the Laplace transform describing $I(t)$. We used a linear least-squares fitting program written by J. R. Winkler subject to a non-negativity restraint in Matlab (Mathworks, Natick, ME). The $P(k_{FET})$ distributions were transformed into $P(R)$ distributions using eq 5:

$$R = \left[\frac{R_o}{\left(\frac{k_{FET}}{k_r}\right)^{1/6}}\right] \quad (5)$$

where k_r is the measured radiative decay rate of apo-GluR2.

RESULTS AND DISCUSSION

Tryptophan Fluorescence and Anisotropy Decay. The four native Trp residues (W460, W671, W766, and W767) are distributed throughout the GluR2 protein, where W460 and W671 are in opposite lobe regions and W766 and W767 are near the hinge region (Figure 1). Collectively, the Trp fluorescence spectrum exhibits a maximum at 325 nm, indicating that the indole side chains are solvent-protected (typical Trp emission in hydrophobic interiors of folded proteins ranges between 308 and 325 nm) (*31*). Using a tryptophan model compound, *N*-acetyl-L-tryptophanamide (NATA) which has a quantum yield of 0.12 (*32*), the relative quantum yield for GluR2 was determined to be 0.64 (on average 0.16, 30% greater per Trp residue than for NATA, [GluR2] = 1 μM in 10 mM HEPES, 20 mM NaCl, 1 mM EDTA, and pH 7.0 buffer). Though GluR2 does contain numerous Tyr residues, their contributions were minimized using an excitation wavelength of 295 nm. To gain further insights into conformational heterogeneity, we have measured the GluR2 Trp fluorescence decay kinetics and ligand binding by time-resolved spectroscopy. Under all solution conditions that were examined ([GluR2] = 0.5−10 μM, pH 7, and [NaCl] = 20−100 mM), we find that there are at least two dominant Trp excited-state decay rates ($k_1 = 2 \times 10^8$ s^{-1}; $k_2 = 3 \times 10^8$ s^{-1}). Despite the widespread use of steady-state emission of the ligand binding domain of GluR2, this is the first report of its time-resolved fluorescence.

Consistent with previously reported steady-state quenching data, in the presence of the glutamate (0.10−1 μM), the average fluorescence lifetime decreases by 10% with the appearance of a new decay rate ($k_3 = 4 \times 10^8$ s^{-1}) and concomitant decrease in the amplitude of k_1. Interestingly, while quenching is observed, the addition of glutamate does not change the spectral properties of the Trp residues. This quenching is due to a dynamic process as evidenced by the decrease in Trp lifetime upon addition of glutamate. It is likely that this change in Trp lifetime is the result of the local conformational changes induced by ligand binding.

To assess the local mobility of the Trp residues in GluR2, we measured the time-resolved fluorescence anisotropy [$r(t)$] in the presence and absence of glutamate (data not shown). Though the majority of Trp fluorescence (>90%) depolarizes within 200 ps, the residual anisotropy [$r(0) = 0.045$] does not depolarize [for L-Trp, the theoretical limit $r(0) = 0.4$] (*33*−*35*) and remains nearly constant during our observation window (~10 ns). Upon

Scheme 1: Structure of the GluR2 Ligands Used in This Study

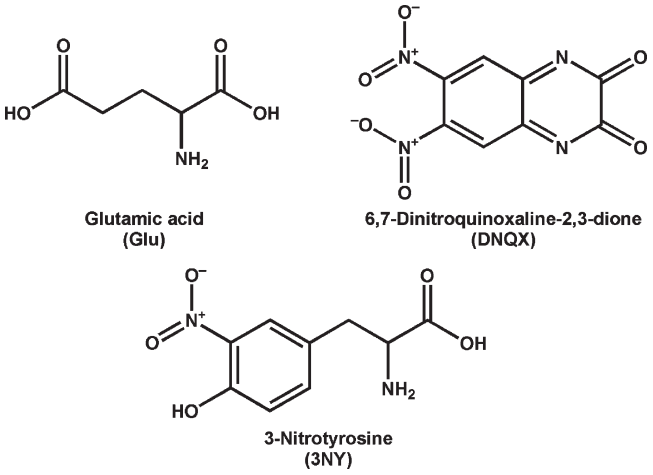

addition of glutamate, the residual anisotropy increases from 0.045 to 0.054; however, we still do not observe any anisotropy decay.

Our time-resolved anisotropy data indicate increased microenvironment viscosity for one or more of the four Trp residues upon glutamate binding. This finding is consistent with those obtained from ^{19}F (5-fluoro-Trp) NMR spectroscopic studies (*7*, *10*) which show that the ligand-bound protein has increased structural rigidity, especially at W671. However, reduced fluorophore mobility would not give rise to the observed quantum yield decrease; restriction of molecular motion (fewer nonradiative deactivation pathways) would rather lead to a fluorescence intensity increase. Additionally, acrylamide quenching experiments have shown that the solvent accessibilities of the Trp residues are not appreciably different between the apo and ligand-bound states, suggesting that the solvent environment is not responsible for fluorescence intensity variations (*20*). It is reasonable to suggest that as GluR2 binds glutamate one of the Trp residues may adopt a local conformation that facilitates other quenching mechanisms such as electron transfer; W767 is a possible candidate because it is in the proximity of the only disulfide bond and Cys 548 (most likely amino acid side chain quenchers) (*36*, *37*). We are unable to directly assess the exact nature of this quenching mechanism because both W766 and W767 are found to be critical for protein stability and folding (*7*); however, Oswald and co-workers found that W767 is sensitive to the relative lobe positions, supporting our notion that this residue may be responsible for the observed quenching.

Transfer of Energy from Trp to DNQX. The interaction between the antagonist, DNQX, and GluR2 has been characterized by X-ray crystallographic (*17*) and NMR spectroscopic studies (*7*, *10*). The crystal structure of GluR2 with DNQX bound is shown in the left panel of Figure 1, with the four native tryptophan residues highlighted in green and distances to DNQX indicated for each Trp residue (15 Å for W460, 20 Å for W671, 17 Å for W766, and 12 Å for W767). Because of the presence of two nitro groups on the quinoxaline ring (Scheme 1), this molecule is a yellow chromophore exhibiting absorption maxima at 355 and 400 nm (molar extinction coefficient of 23400 M^{-1} cm^{-1} at 355 nm). As anticipated, the DNQX spectroscopic feature makes it a suitable energy acceptor for Trp emission (Figure 2). Using the Förster equations (Data Analysis, eqs 2 and 3), we calculate the corresponding R_o to be 33 Å, allowing the determination of donor−acceptor distances of 20−50 Å. On the

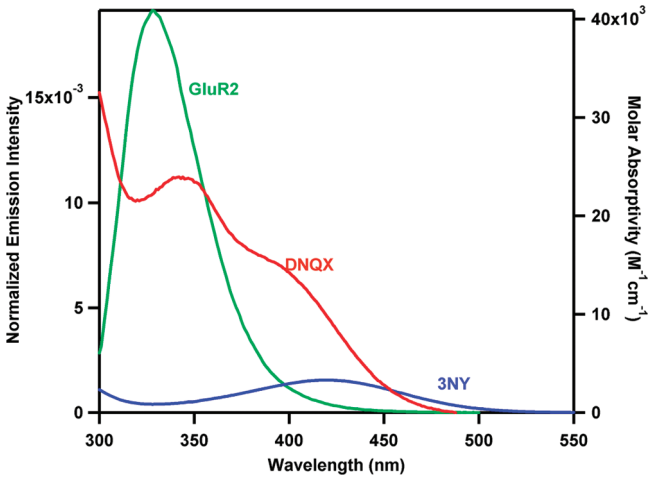

FIGURE 2: Spectral properties of fluorescence energy transfer ligand probes, 6,7-dinitroquinoxaline-2,3-dione (DNQX) and 3-nitrotyrosine (3NY). Spectral overlap of the Trp fluorescence spectrum of GluR2 (green) and the absorption spectra of DNQX (red) and 3NY (blue).

basis of the average crystallographically determined Trp−DNQX distance of ~16 Å, FET will occur from all of the Trp residues in GluR2 to DNQX, resulting in fluorescence quenching upon antagonist binding.

Using both steady-state and time-resolved Trp fluorescence measurements, we monitored DNQX binding. Addition of DNQX to a solution of GluR2 results in dramatic quenching of the tryptophan emission ([GluR2] = [DNQX] = 1 μM, 60% quenching), consistent with FET occurring from tryptophan to DNQX. Clearly, the Trp fluorescence lifetime of GluR2 decreases in the presence of DNQX, verifying the occurrence of FET (Figure 3A). We observe substantial FET between Trp residues in GluR2 and DNQX; these rates approach the instrument response function (~500 ps) under our current measurement conditions. Taking this into consideration, we have restricted the fastest rate in our fits (see Data Analysis) to 2×10^9 s^{-1} and categorized our rates into two populations: DNQX−GluR2 complex ($k_{FET} > 1 \times 10^9$ s^{-1}) and apo-GluR2 (intrinsic rates of $< 1 \times 10^9$ s^{-1}). The relative amplitudes are plotted as a function of DNQX concentration (Figure 3A, inset). Although the relative amplitudes and rate constants can vary slightly for different titrations, similar trends were always observed: increase in the DNQX-GluR2 population with a concomitant decrease in the apo-GluR2 population as a function of added DNQX. From peak-normalized decay curves, we obtained an apparent dissociation constant (K_d) of 0.6(1) μM for the GluR2−DNQX complex, comparable to the submicromolar dissociation constant reported by Oswald and co-workers (Figure 4) (*10*).

Due to the existence of multiple donor fluorophores (Trp), we elected to estimate an average donor−acceptor separation ($\langle R_{DA} \rangle$) from the FET rates to compare with those measured in the crystal structure. The distance we calculate is 24 Å, whereas the Trp−DNQX separations for all four Trp residues in the crystal structure are ≤20 Å (Figure 1, left panel). The slight elongation of our $\langle R_{DA} \rangle$ may reflect dynamical properties of the protein in solution. Alternatively, the expected distances are near the limit of the distances we can expect to resolve, and the actual distances are, in fact, shorter.

3-Nitrotyrosine, a New FET Ligand. On the basis of the structures of known ligands for GluR2, many of which contain

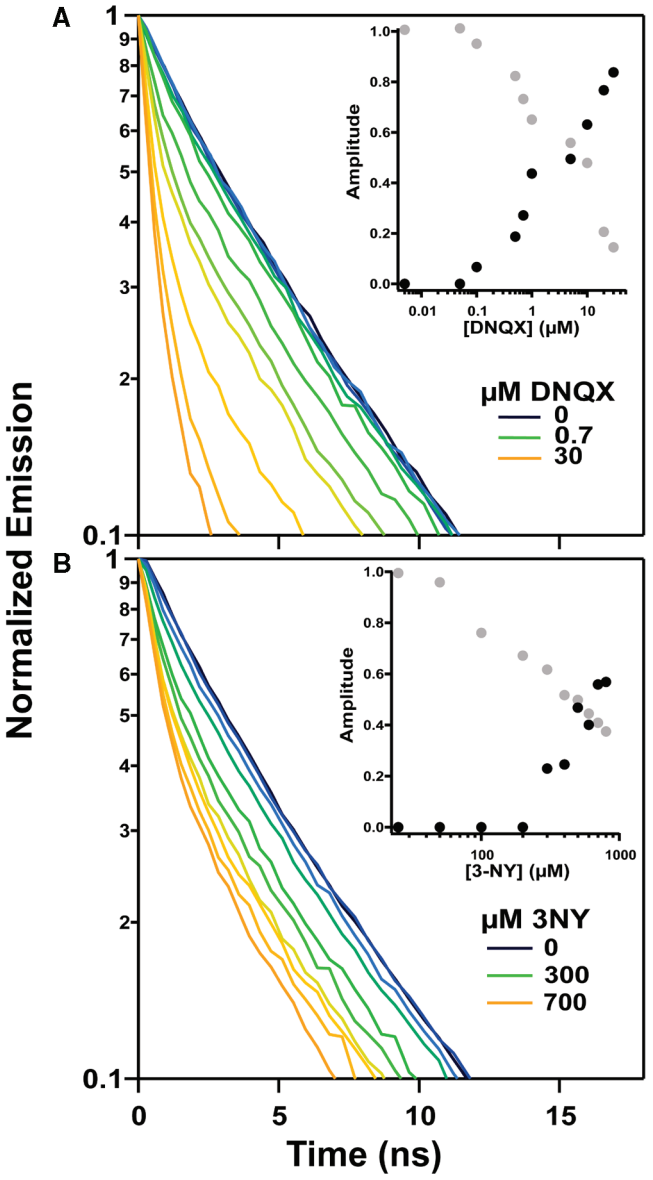

FIGURE 3: Tryptophan fluorescence decay kinetics of GluR2 with increasing concentrations of DNQX (0.25−30 μM) (A) and 3NY (25−700 μM) (B) from blue to orange. The insets show the relative amplitudes of the rate constants [apo-GluR2 (gray circles) and ligand-bound GluR2 (black circles)] extracted from NNLS fits of Trp fluorescence decay curves as a function of ligand concentration.

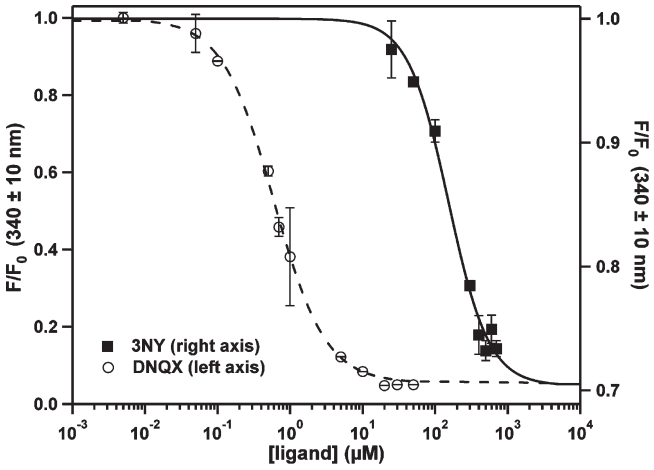

FIGURE 4: Ligand titration curves obtained by time-resolved Trp fluorescence. Addition of increasing concentrations of DNQX (○, left axis) and 3NY (■, right axis) to 1 μM GluR2 in 10 mM HEPES and 20 mM NaCl buffer (pH 7.0) results in quenching of Trp fluorescence by binding of the energy transfer ligands. Lines represent fits.

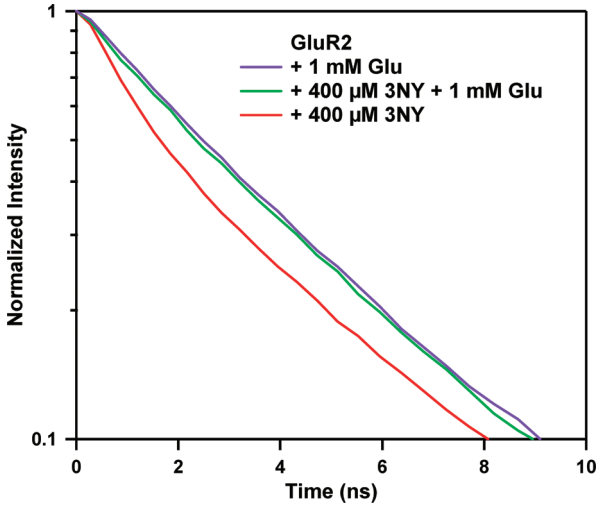

FIGURE 5: Specificity of 3NY for the glutamate ligand binding pocket is demonstrated by the ability of glutamate to displace 3NY. With 3NY bound to the protein, the tryptophan fluorescence is quenched by FET to 3NY (red trace). Addition of glutamate results in recovery of the tryptophan fluorescence (green trace), indicating the displacement of 3NY from the ligand binding site.

the essential amino acid functional groups (α-amino and carboxyl group) (Scheme 1) and the spectroscopic properties of a chemically modified tyrosine (λ_{max} = 420 nm, pH 7.0), we hypothesized that 3-nitrotyrosine (3NY) would be a potential FET ligand (calculated $R_o \sim 24$ Å) for GluR2 (Figure 2). Indeed, 3NY does bind to GluR2 but with a considerably reduced affinity compared to that of DNQX (Figures 3 and 4). Tryptophan emission quenching is observed only at a 3NY:protein stoichiometry of >10:1. Because of the apparent low affinity of the 3NY−GluR2 complex, the increased concentrations of 3NY present a substantial inner filter effect on the steady-state fluorescence measurement. To reliably extract the K_d, we turned to time-resolved Trp fluorescence measurements to obtain Trp-to-3NY FET rates (Figure 3B). These measurements revealed one dominant rate ($k_{FET1} = 1 \times 10^9$ s^{-1}) and a minor rate ($k_{FET2} = 4 \times 10^8$ s^{-1}). The relative amplitude of k_{FET1} is highly dependent on the concentration of 3NY attributable to FET from Trp to 3NY that occurs upon specific binding of 3NY in the ligand pocket. In contrast, the amplitude of k_{FET2} does not depend on the concentration of 3NY in solutions. Similar to the DNQX titration, we observe the apo-GluR2 population decreasing as the ligand is added. Our data can be adequately fit to a single-site binding model with an apparent K_d of ~170(30) μM (Figure 4). The $\langle R_{DA} \rangle$ values we calculate from these rates are 18 and 24 Å, which are comparable to the distance that we estimated for DNQX−GluR2 complex. Despite the inherent uncertainty in our estimation of the orientation factor (κ^2), our data suggest that the clamshell closes around 3NY more tightly than DNQX. Using the empirically determined relationship between the "openness" of the cleft and ligand pharmacology, we predict that 3NY would have antagonist activity. Preliminary electrophysiology experiments with the full-length receptor do suggest that 3NY is a very weak antagonist.

The specificity for the ligand binding cleft is shown by competition using glutamate (Figure 5). Upon the addition of

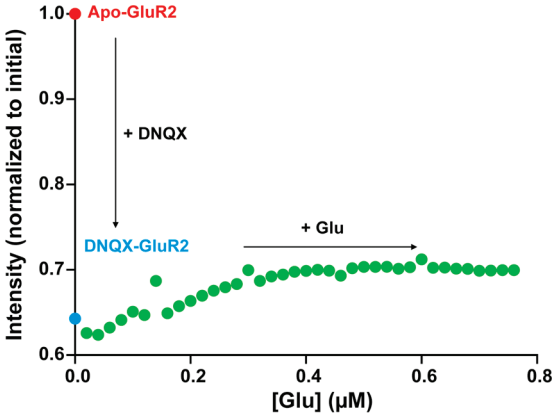

FIGURE 6: Competitive binding assay in which varying concentrations of glutamate are added to a solution of 1 μM GluR2 and 1 μM DNQX. The first point is the emission intensity of 1 μM GluR2 before addition of DNQX to a final concentration of 1 μM. As glutamate displaces DNQX in the ligand binding site, the tryptophan fluorescence intensity increases.

glutamate, the fluorescence quenching was recoverable, nearly identical to the independently measured kinetics for the GluR2−glutamate complex indicating that the glutamate is displacing 3NY from the ligand binding cleft. Moreover, control experiments were conducted using a model fluorophore, NATA and 3NY, to examine any presence of bimolecular (collisional) quenching; the excited-state decay kinetics are identical for NATA in buffer and in a solution containing 700 μM 3NY. We also confirmed that an analogous compound, 3-iodotyrosine, a close contact quencher (due to the presence of the iodo group), does not affect GluR2 fluorescence further, providing evidence that the dynamic quenching is attributable to FET.

DNQX in a Competitive Ligand Assay. Though radioligand assays are commonly used as the current standard for sensitivity in GluR2 competitive ligand binding detection, fluorescence-based methods can permit detection of ligands without the safety and environmental issues concerning radioactivity. Since we have identified DNQX as an efficient FET acceptor ligand, we have furthered this study to demonstrate its utility as a FET competitor. Displacement of the FET acceptor ligand (DNQX) from the binding site by another ligand (glutamate) results in "turning on" the Trp emission; indeed, this offers an alternative competitive ligand assay (Figure 6). Interestingly, we find that glutamate cannot fully displace DNQX as evidenced by a lack of total fluorescence recovery. This observation was somewhat unexpected because to the best of our knowledge there are no reports of irreversible binding of DNQX to GluR2. While the apparent irreversible DNQX binding may prove to be problematic especially for quantitative K_d determinations (an evidently higher K_d of ~2 μM for glutamate), the methodology using FET ligands and intrinsic Trp fluorescence is broadly applicable for protein−ligand interactions.

CONCLUSION

Using time-resolved fluorescence and anisotropy measurements, we characterized the excited-state properties and local mobility of Trp residues in the isolated LBD, GluR2. The FET acceptor ligands that we identified, DNQX and 3NY, both bind specifically to the ligand binding cleft of GluR2. Upon binding, these ligands are stabilized within Förster's radius of all four native tryptophan residues and act as efficient FET acceptors. Interestingly, we observe multiple rate components for 3NY suggestive of ligand−protein complex structural heterogeneity. However, due to the presence of multiple Trp donors, we are able to estimate only average DNQX−3NY distances to the Trp residues. While the distance extracted (24 Å) from our analysis on the DNQX−Trp GluR2 complex is on the order of the crystallographically determined distances (12−20 Å), they are somewhat longer. This may be due to the current limit of resolvable rates ($k \geq 2 \times 10^9$ s^{-1}) which would correspond to donor−acceptor distances shorter than those estimated for Trp-DNQX, or it is possible that it is attributable to unfavorable orientations of the Trp and DNQX transition dipoles in the folded protein. Alternatively, our longer distances may simply reflect dynamical properties of the protein in solution.

While DNQX is a well-known complex, its spectroscopic properties and potential application as a sensitive reporter for binding of the ligand to GluR2 have been overlooked previously. We have described a DNQX competition assay that represents a significant improvement over the fluorescence assays currently in use in that this is a "turn-on" sensor, eliminating false positive observations inherent to quenching events resulting from photobleaching. The use of FET competitor ligands and intrinsic Trp fluorescence should allow for the future identification of novel ligands not only for GluR2 but also for other proteins when DNQX or structural analogues (i.e., CNQX and other nitrated aromatic compounds) are employed.

ACKNOWLEDGMENT

We thank Mark L. Mayer (The Eunice Kennedy Shriver National Institute of Child Health and Human Development, National Institutes of Health) for performing electrophysiology experiments using 3-nitrotyrosine, Thai Leong Yap for assistance in protein purification, Eric Gouaux (The Vollum Institute, Oregon Health & Science University) for providing the expression plasmid and purification protocol, and Jay R. Winkler (Beckman Institute Laser Resource Center, California Institute of Technology, Pasadena, CA) for providing the fitting routines used for the time-resolved fluorescence analyses.

REFERENCES

1. Dingledine, R., Borges, K., Bowie, D., and Traynelis, S. F. (1999) The glutamate receptor ion channels. *Pharmacol. Rev. 51*, 7–62.
2. Madden, D. R. (2002) The structure and function of glutamate receptor ion channels. *Nat. Rev. Neurosci. 3*, 91–101.
3. Malenka, R. C., and Nicoll, R. A. (1999) Long-term potentiation: A decade of progress? *Science 285*, 1870–1874.
4. Mead, A. N., and Stephens, D. N. (2003) Involvement of AMPA receptor GluR2 subunits in stimulus-reward learning: Evidence from glutamate receptor gria2 knock-out mice. *J. Neurosci. 23*, 9500–9507.
5. Beal, M. C. (1992) Mechanisms of excitotoxicity in neurologic diseases. *FASEB J. 6*, 3338–3344.
6. Dingledine, R., McBain, C. J., and McNamara, J. O. (1990) Excitatory amino acid receptors in epilepsy. *Trends Pharmacol. Sci. 11*, 334–338.
7. Ahmed, A. H., Loh, A. P., Jane, D. E., and Oswald, R. E. (2007) Dynamics of the S1S2 glutamate binding domain of GluR2 measured using F-19 NMR spectroscopy. *J. Biol. Chem. 282*, 12773–12784.
8. Chen, G.-Q., and Gouaux, E. (1997) Overexpression of a glutamate receptor (GluR2) ligand binding domain in *Escherichia coli*: Application of a novel protein folding screen. *Proc. Natl. Acad. Sci. U.S.A. 94*, 13431–13436.
9. Valentine, E. R., and Palmer, A. G. (2005) Microsecond-to-millisecond conformational dynamics demarcate the GluR2 glutamate receptor bound to agonists glutamate, quisqualate, and AMPA. *Biochemistry 44*, 3410–3417.
10. Ahmed, A., Thompson, M., Fenwick, M., Romero, B., Loh, A., Jane, D., Sondermann, H., and Oswald, R. (2009) Mechanisms of

antagonism of the GluR2 AMPA receptor: Structure and dynamics of the complex of two willardiine antagonists with the glutamate binding domain. *Biochemistry 48*, 3894–3903.
11. Ramanoudjame, G., Du, M., Mankiewicz, K. A., and Jayaraman, V. (2006) Allosteric mechanism in AMPA receptors: A FRET-based investigation of conformational changes. *Proc. Natl. Acad. Sci. U.S.A. 103*, 10473–10478.
12. Du, M., Reid, S. A., and Jayaraman, V. (2005) Conformational changes in the ligand-binding domain of a functional ionotropic glutamate receptor. *J. Biol. Chem. 280*, 8633–8636.
13. Abele, R., Keinanen, K., and Madden, D. R. (2000) Agonist-induced isomerization in a glutamate receptor ligand-binding domain: A kinetic and mutagenetic analysis. *J. Biol. Chem. 275*, 21355–21363.
14. Hogner, A., Kastrup, J. S., Jin, R., Liljefors, T., Mayer, M. L., Egebjerg, J., Larsen, I. K., and Gouaux, E. (2002) Structural basis for AMPA receptor activation and ligand selectivity: Crystal structures of five agonist complexes with the GluR2 ligand-binding core. *J. Mol. Biol. 322*, 93–109.
15. Jin, R. S., and Gouaux, E. (2003) Probing the function, conformational plasticity, and dimer-dimer contacts of the GluR2 ligand-binding core: Studies of 5-substituted willardiines and GluR2 S1S2 in the crystal. *Biochemistry 42*, 5201–5213.
16. Armstrong, N., and Gouaux, E. (2000) Mechanisms for activation and antagonism of an AMPA-sensitive glutamate receptor: Crystal structures of the GluR2 ligand binding core. *Neuron 28*, 165–181.
17. Kasper, C., Pickering, D. S., Mirza, O., Olsen, L., Kristensen, A. S., Greenwood, J. R., Liljefors, T., Schousboe, A., Watjen, F., Gajhede, M., Sigurskjold, B. W., and Kastrup, J. S. (2006) The structure of a mixed GluR2 ligand-binding core dimer in complex with (S)-glutamate and the antagonist (S)-NS1209. *J. Mol. Biol. 357*, 1184–1201.
18. Holm, M. M., Lunn, M. L., Traynelis, S. F., Kastrup, J. S., and Egebjerg, J. (2005) Structural determinants of agonist-specific kinetics at the ionotropic glutamate receptor 2. *Proc. Natl. Acad. Sci. U.S.A. 102*, 12053–12058.
19. Stoll, L., and Gentile, L. (2005) Linking tricyclic antidepressants to ionotropic glutamate receptors. *Biochem. Biophys. Res. Commun. 333*, 622–627.
20. Stoll, L., Hall, J., Van Buren, N., Hall, A., Knight, L., Morgan, A., Zuger, S., Van Deusen, H., and Gentile, L. (2007) Differential regulation of ionotropic glutamate receptors. *Biophys. J. 92*, 1343–1349.
21. Eftink, M. R. (1991) Fluorescence Techniques for Studying Protein Structure. In Methods of Biochemical Analysis: Protein Structure Determination (Suelter, C. H., Ed.) pp 127−205, John Wiley & Sons, Inc., New York.
22. Beechem, J. M., and Brand, L. (1985) Time-resolved fluorescence of proteins. *Annu. Rev. Biochem. 54*, 43–71.
23. Callis, P. R. (1997) L-1(a) and L-1(b) Transitions of Tryptophan: Applications of Theory and Experimental Observations to Fluorescence of Proteins. In Fluorescence Spectroscopy, pp 113−150, Academic Press Inc., San Diego.
24. Navon, A., Ittah, V., Landsman, P., Scheraga, H. A., and Hass, E. (2001) Distribution of intramolecular distances in the reduced and denatured states of bovine pancreatic ribonucleases A. Folding initiation structures in the C-terminal portions of the reduced protein. *Biochemistry 40*, 105–118.
25. Rischel, C., Tyberg, P., Riglere, R., and Poulsen, F. M. (1996) Time-resolved fluorescence studies of the molten globule state of myoglobin. *J. Mol. Biol. 257*, 877–885.
26. Lee, J. C., Langen, R., Hummel, P. A., Gray, H. B., and Winkler, J. R. (2004) α-Synuclein structures from fluorescence energy transfer kinetics: Implications for the role of the protein in Parkinson's disease. *Proc. Natl. Acad. Sci. U.S.A. 101*, 16466–16471.
27. Hartings, M. R., Gray, H. B., and Winkler, J. R. (2008) Probing melittin helix-coil equilibria in solutions and vesicles. *J. Phys. Chem. B 112*, 3202–3207.
28. Wu, P. G., and Brand, L. (1994) Resonance energy transfer: Methods and applications. *Anal. Biochem. 218*, 1–13.
29. Brand, L., and Gohlke, J. R. (1972) Fluorescence probes for structure. *Annu. Rev. Biochem. 41*, 843–868.
30. Beechem, J. M., and Hass, E. (1989) Simultaneous determination of intramolecular distance distributions and conformational dynamics by global analysis of energy transfer measurements. *Biophys. J. 55*, 1225–1236.
31. Lakowicz, J. R. (2006) Principles of Fluorescence Spectroscopy, 3rd ed., Springer, Berlin.
32. Chen, R. (1972) Measurements of absolute values in biochemical fluorescence spectroscopy. *J. Res. Natl. Bur. Stand. (U.S.) 76A*, 593–606.
33. van den Berg, R., Jang, D. J., and el-Sayed, M. A. (1990) Decay of the tryptophan fluorescence anisotropy in bacteriorhodopsin and its modified forms. *Biophys. J. 57*, 759–764.
34. Nordlund, T. M., and Podolski, D. A. (1983) Streak camera measurement of tryptophan and rhodamine motions with picosecond time resolution. *Photochem. Photobiol. 38*, 659–664.
35. Ruggiero, A. J., Todd, D. C., and Fleming, G. R. (1990) Subpicosecond fluorescence anisotropy studies of tryptophan in water. *J. Am. Chem. Soc. 112*, 1003–1014.
36. Chen, Y., and Barkley, M. D. (1998) Toward understanding tryptophan fluorescence in proteins. *Biochemistry 37*, 9976–9982.
37. Adams, P. D., Chen, Y., Ma, K., Zagorski, M. G., Soonichsen, F. D., McLaughlin, M. L., and Barkley, M. D. (2002) Intramolecular quenching of tryptophan fluorescence by the peptide bond in cyclic hexapeptides. *J. Am. Chem. Soc. 124*, 9278–9286.
38. Chen, G.-Q., Sun, Y., Jin, R., and Gouaux, E. (1998) Probing the ligand binding domain of the GluR2 receptor by proteolysis and deletion mutagenesis defines domain boundaries and yields a crystallizable construct. *Protein Sci. 7*, 2623–2630.